IEEE Access
Multidisciplinary | Rapid Review | Open Access Journal

Received June 4, 2020, accepted June 10, 2020, date of publication June 16, 2020, date of current version June 29, 2020.

Digital Object Identifier 10.1109/ACCESS.2020.3002685

Towards an All-Wheel Drive Motorcycle: Dynamic Modeling and Simulation

ANDREA BONCI, (Member, IEEE), SAURO LONGHI, (Senior Member, IEEE), AND GIUSEPPE ANTONIO SCALA

Dipartimento di Ingegneria dell'Informazione (DII), Università Politecnica delle Marche, 60131 Ancona, Italy

Corresponding author: Andrea Bonci (a.bonci@univpm.it)

This work was supported in part by the EU H2020 ENCORE Project "Energy aware BIM Cloud Platform in a COst-effective Building Renovation Context", European Union's Horizon 2020 research and innovation programme under Grant Agreement No 820434, in part by the REACT Project "Methods and innovative instruments for REACTive Product Design and Manufacturing", Project from the Italian Ministry of University and Research (MIUR)-in National Operative Plan (PON) for Research and Innovation 2014-2020, Project No ARS01_01031, Grant Agreement D.D. July 13 2018, n. 1825-Code ARS01_01031, and in part by the HD3Flab Project "Human Digital Flexible Factory of the Future Laboratory" EU ERDF (European Regional Development Fund), Regional Operative Plan (POR) MARCHE Region FESR (Fondo Europeo di Sviluppo Regionale) 2014/2020, AXIS 1, Specific Objective 2, ACTION 2.1.

ABSTRACT Modern motorcycles are evolving more and more towards complex systems by the increasing integration of mechanical, electrical and control disciplines. All-wheel drive (AWD) vehicles have proven effective to improve vehicle's performances and rider's safety. Despite this, manufacturers have developed few AWD motorcycles and little research has been devoted to them. Obvious difficulties concern torque distribution to the front wheel because of steering system. Nowadays, the integration of technologies eases the implementation of front wheel drive opening new research perspectives. In this work, the dynamic model of an AWD motorcycle with an attached rider is proposed. It represents the first symbolic analysis investigating the effects of front wheel traction on the dynamics of a motorcycle for supporting the design of AWD motorcycles reducing trials and tests on prototypes. The proposed model is parametric with respect to the motorcycle geometry, and it allows to simulate complex operating modes of the AWD, such as cornering phenomena, taking into account coupling of lateral and longitudinal dynamics and tire-road interactions. Unlike other works, here the authors include a full tire model by exploiting theoretical slips of the brush model for tire's aligning moment too, instead of applying a totally empirical representation less suitable for a complete symbolic description. Besides, to simulate the equations of motion, the benefits and disadvantages of using AWD with torque distribution have been pointed out introducing a new handling ratio. Two verification procedures validate the model: one is performed theoretically, the other carries out a comparison with a multibody software, whose model is more sophisticated, this latter embeds all main motorcycle's dynamics. Although radically different, being the first theoretical and the second numerical-computational, both methods exhibit consistent behavior between them, and effectiveness of the former is also consistent with the results of a multibody simulator under the assumptions made.

INDEX TERMS Vehicle dynamics, modeling, simulation, intelligent transportation systems, road vehicles.

I. INTRODUCTION

During the last decades, despite a few motorcycle producers have spent efforts into proposing solutions to front wheel drive of AWD motorcycles [1]–[3], researches on the topic are still lacking. Although different solutions have been developed and even more can be foreseen by using electric propulsion, these commercial AWD vehicles have all been conceived to overcome conditions of low traction due to sandy or rough terrains. They use hydraulic or mechanical driveline to transfer a fixed portion of the drive torque to the front wheel permanently or else when excessive slip at rear wheel arises. These vehicles do not fully exploit the factual potential of AWD motorcycle. Being not conceived for smart management of the drive torque, they are unable to adapt the latter between both wheels in several complex dynamic conditions. Modulating torque distribution between wheels will give the designer more control over vehicle's performances and handling characteristics; this will be proven in the paper in a simulation scenario, in which analysis of a typical cornering maneuver will show how the AWD advantages and drawbacks could be enhanced and mitigated, respectively,

The associate editor coordinating the review of this manuscript and approving it for publication was Fabrizio Messina.

by torque modulation between wheels. Benefits of traction available at the normally undriven wheel improve acceleration and stability in cornering, reduces the tendency of the rear wheel to slip and applies useful drive in the direction the rider wants to go. Evidences of experienced riders point out these features. The availability of suitable mathematical tools able to capture and describe these phenomena would facilitate engineering development of such vehicles and migration towards these new traction solutions. This work aims at being the first step of a broader research work, which develops a model that can lay the foundations for subsequent investigations of suitable control techniques from which the AWD can benefit. Here, such a mathematical model has been developed for supporting the design and analysis of two-wheeled vehicles that intend to take advantage of AWD features and to reduce trials and tests on prototypes. Regarding technical solutions to deploy AWD potential, the electric wheel drive could help migration towards full AWD exploitation. It is becoming more appealing not only for cars but also for two-wheeled vehicles. Nowadays, small and powerful motors can be housed in the vehicle wheel assemblies bringing undoubted benefits such as precise and quick torque response, accurate drive torque control and the possibility of getting helpful information on the wheel angular velocity and torque by measuring the electric current absorbed by the motor. Despite technological advances, at present AWD motorcycles design still seems to rely on experience rather than on an understanding of its phenomena, which instead would allow a factual success. Before moving from an idea to a prototype and then to a product, development of newly conceived vehicle requires an in-depth investigation of its distinguishing dynamics to cope in advance with limits and strengths. This requires high-fidelity dynamic model able to reproduce, although with approximations, the real vehicle over normal operating conditions. Once available the equations governing the system, by focusing on specific modeled dynamics, a suitably control-oriented model could be arranged, facilitating model-based control with the purpose of directly influence vehicle dynamics not only by steering control but also through the torque distribution between wheels. This offers to the designer more degrees of freedom to influence the handling, the driving comfort and safety in a variety of conditions and situations, thus relegating the necessity for expensive empirical testing only to the validation phase. This paper addresses the issue of defining a viable symbolic model for describing an AWD motorcycle's behavior subject to torque distribution in different driving conditions. The model is generally valid, namely it has been developed regardless of the adopted driveline technology for the torque distribution to the front wheel. To strengthen model reliability, two verification procedures are adopted to validate it. The first one validates theoretically the symbolic model in steady-state cornering condition. The second one, relies on multibody analysis, which as a matter of fact in the automotive field is reputed by now as a de-facto standard, suitable to simulate the tests and the behaviors that a real prototype would be subject to during the development as a new product [4]; hence, the model behavior has been further compared with a most realistic multibody-simulator, developed in MSC Adams, richer in terms of dynamics, rigid bodies and degrees of freedom. The symbolic model shows consistent behavior with the multibody simulator under the assumptions made. Finally, the benefits and disadvantages of using AWD with torque distribution have been analyzed. The paper is organized as follows: Section 2 introduces the related work; Section 3 and 4 are devoted to describing the AWD symbolic model. Section 5 describes the adopted tire's model. Section 6 introduces the multibody model, Section 7 is focused on the theoretical validation of the model, Section 8 shows comparative simulation and results. Section 9 concludes the paper.

II. RELATED WORK

Over the years, many efforts have been devoted to developing two-wheeled vehicles (2WVs) with rear wheel drive. The joint progress between industrial development and mathematical models' analysis had led to a meaningful technological evolution of the 2WVs. The same did not happen for the AWD version of these vehicles, as instead occurred for cars. The reasons are twofold, technological and theoretical. To understand them better, in the following it will be introduced both the few industrial developments of AWD motorcycles and the main theoretical progress of the 2WVs, up to the AWD counterpart. The idea of AWD is not new in the field of motorcycles, indeed some early implementations of all-terrain vehicle date back to the 60s, see e.g. the Rokon motorcycles [1]. Then later over the years, some prototypes have been developed. However, only few commercial proposals have been made, mostly involving internal combustion engine (ICE) and with obvious mechanical difficulties in distributing the torque through the front wheel. Without going into details of all the prototypes, we will briefly mention few notable products that have had commercial implications together with their main features. Rokon manufacturer is a long-time producer of AWD motorcycles. They are off-road and low speed motorcycles designed for use in the most rugged terrain. Rokon uses ICE of about 6 Hp and a combination of belt, chain and shaft drives coupled to gear boxes to drive both front and rear wheel. Back in the early 90s, Swedish suspension specialists Öhlins [2] started working on a two-wheel drive system for the Japanese manufacturer Yamaha. The system is based on a hydraulic pump driven by the engine in the rear frame which forces oil in hoses to a small hydraulic motor in the front wheel. It activates in slip condition of the rear wheel; during this, the hydraulic pump transfers the exceeding energy of the spinning tire to the hydraulic motor of the front wheel by generating a smooth transmission torque. It involves an additional weight of about 8 kg. In 2004 Yamaha produced in limited numbers the WR450 2-Trac off-road motorbike. In the same years the two-wheel drive set-up from Öhlins has been deployed on the Yamaha R1 sportbike. Another noteworthy manufacturer is

the US firm Christini [3], it offers two-wheel drive conversions to experience the AWD for off-road bikes and military applications. The Christini's AWD system delivers power from the motorcycle transmission to the front wheel through a series of chains and shafts, it is complicated, but it is also fairly light and can be applied to several bikes. The transferred torque is predefined by design. The front wheel engages with the drive system and starts to pull as soon as the rear loses traction. The above models have not been conceived to adapt the drive torque between both wheels in several dynamic conditions without slip arising. Besides, a theoretical analysis did not follow jointly their development, probably because of the need to investigate behaviors mainly under slip conditions. Conversely, over the years this has not happened for the 2WVs, for whom many efforts have been devoted to dynamic modeling and analysis. In this regard, the paper of Limebeer and Sharp [5] represents a milestone about the development of the subject concerning single track vehicles modeling and control. They explored the subject since the mid-1850s when the landmark publications started to appear, and the references therein also provide a comprehensive review concerning motorcycles, ranging from pioneering and simple models to more detailed ones. For the sake of brevity, only a few of many noteworthy works in [5] will be mentioned below, the reader can refer to [5] for further details. Dates back to the '70s the influential work of Sharp [6] to the theoretical analysis of motorcycle in straight-running. A linearized model with minimum complexity that included for the first time simplified tire-road interaction without aerodynamic effects and suspension motions had been investigated for lateral stability analysis together with influences of parameter uncertainties on the stability. In the same years was shown the importance of aerodynamic forces on the performance and stability of motorcycles [7]. Some years later the same Sharp [8] tries to investigate the effects of acceleration and deceleration on motorcycles' stability with a rather simplified approach introducing longitudinal equation of motion decoupled from the lateral equations. Some decades later, in [9] those conclusions were partially refuted by using a higher fidelity multibody model but influence of acceleration or braking on a cornering machine is still an open issue. During '90s extensive use of multibody simulators to evaluate the performance of motorcycles has started [10], [11], besides was laid the foundations of motorcycle's tire modeling [12], [13]. In the following decade the contemporary empirical tire models for motorcycles was developed [14]. A comprehensive overview of many of these models is given in [15]. During the '2000s, Cossalter and Lot [16] present a motorcycle model described as a set of 6 bodies for FastBike simulation program. The literature concerning the stabilization of 2WV is quite recent [17], [18], a double loop controller is generally proposed to follow a road path pre-computed by strategies such as the optimal maneuver method [19]. Later, Kooijman and Schwab [20] have presented a wide review on bicycle and motorcycle rider control. More recently for simulator application a motorcycle dynamic model was derived by using a recursive Newton-Euler [21], whereas in [22] an alternative modeling approach based on the Jourdain's principle is presented to derive a mathematical description of a motorcycle vehicle; finally, more recently in [23] it has been shown as the roll angle linearization assumption could be removed from rear wheel drive motorcycle models and it has been used for investigating critical motorcycle's falls, such as the low side fall. As showed by the above overview, the 2WVs has reached maturity in addressing many dynamic aspects. By focusing instead on AWD motorcycle, at best of authors' knowledge, a noteworthy multibody model is proposed in [24] where the authors analyze some handling characteristics as well as the energy efficiency achievable by using the torque distribution, this work shows as torque distribution does not provide significant improvement in terms of energy saving, on the other hand it gives some clues on good handling characteristics of an AWD vehicle negotiating a cornering. While the dynamics of 2WVs has been investigated by means of the symbolic model formulation [25] or by computer assisted multibody modeling (which overcomes the difficulties in handling complex symbolic equations), AWD dynamics still appears to be in the early stage. For this topic indeed few existing works exploit simple AWD models with one rigid body, e.g. in [26] it has been proposed the AWD slip control in presence of roll angle. However, a single rigid body model is not suitable to investigate more complex dynamics of AWD vehicle, and a more accurate model is advisable. A work addressing practical low-cost solutions for the automatic engagement of the front wheel drive in an AWD motorcycle can be found in [27]. In this general context, our aim is to find a proper mathematical representation of the motorcycle which describes the essential dynamics issues of the AWD. The model is intended to facilitate the vehicle's dynamics control through the torque distribution between wheels.

III. AWD MOTORCYCLE MODELING

In this section, the model of AWD motorcycle is proposed in terms of a set of symbolic equations of motion (EOMs), derived by using Lagrangian formulation. Generally, this provides fully nonlinear EOMs having higher complexity of expressions and wide operating range. Approaching the analysis of newly conceived vehicle, rather than a full complexity model, firstly requires investigation of its distinguishing dynamics, albeit complex, over limited operating conditions even with approximated models, as shown by vast literature [6], [28], [29]. Accordingly, by focusing here on certain basic operating conditions, is advisable to avoid the wide range of vehicle's trim conditions linked to a complex model. Subsequently, once verified the model's effectiveness in conditions deemed basic, the roll angle linearization assumption could be removed to widen the operating range focusing on higher performance of the vehicle, as already showed in [23], [30] for the investigation of rear wheel drive motorcycle's falls. This would open the way to a further novel result consisting of a symbolic model linearized around non-zero

trim condition and parameterized with respect to the roll angle, thus would allow it to perform a steady turning analysis at higher performance and investigate on suitable controllers. Currently this was attempted with black-box approaches on rear wheel drive vehicles by acquiring the vehicle's frequency response in steady turning condition from multibody simulator, by assuming that it can reproduce realistic dynamics of the vehicle [31], [32]. The present paper focuses on the dynamic model of AWD motorcycle able to describe its basic and distinguishing dynamics; it represents the first stage of the path above mentioned for developing newly conceived AWD vehicles. As first attempt of analysis of AWD vehicles, the vertical trim condition has been chosen, afterwards, excessive lean angles in cornering have been avoided by means of a virtual rider controller. Thus, nonlinear EOMs have been linearized about the vertical position. The contributions of this work are different, firstly it proposes a parametric model having the lowest allowed complexity, able to describe with enough accuracy the dynamics of AWD vehicle in complex operating modes such as cornering phenomena, taking into account coupling of lateral and longitudinal dynamics and the tire-road interactions. Besides, it shows how to integrate into AWD symbolic model a full tire model by exploiting theoretical slips of the brush model for tire's aligning moment too, instead of applying totally empirical model less suitable for the symbolic modeling. In addition to simulate equations of motion, the model has proven to be effective in highlighting effects of the front wheel drive on motorcycle's dynamics allowing to describe the benefits and disadvantages of using AWD with torque distribution.

The tires model plays a major role in motorcycle modeling, in this regard a specific section will be devoted to describe a proper model and its integration with the symbolic environment to provide the expressions of the contact forces and the contact moments acting on the tires.

A. ASSUMPTIONS AND NOTATIONS

The model derivation makes the following assumptions:

- the motorcycle moves on a flat road surface and the vertical dynamics and the effects of the suspensions system have been neglected. Accordingly, it will be deemed acceptable for our purposes those traction torques avoiding abrupt vehicle's accelerations, so that no excessive fore-and-aft load transfer is triggered. Also, the motorcycle tricky phenomena such as the wheelie and the stoppie are out of the scope of the paper;
- the rider has been modeled as a body rigidly attached to the rear frame;
- the direction and the velocity of the motorcycle is controlled by the rider acting on the steering mechanism and on the front and rear engine torques;
- the contact forces and moments are accounted as external forces generated by a specific tire-road interaction model.

The motorcycle's geometry is shown in Fig. 1. It consists of two rigid bodies, the front and the rear one. From now on in the paper the subscript $i \in \{r, f\}$ will refer to the rear and the front body respectively. The rear frame, represented by its center of mass G_r includes the rear engine, the propellant storage, either the petrol tank or the battery storage, the saddle, the rear wheel with radius R_r and the rider. The front frame is represented by its center of mass G_f, it is constrained to the rear frame by means of a revolute joint, it includes the front engine, the handlebars, the fork, the steering mechanism and the front wheel with radius R_f. Furthermore, Fig. 1 shows the vertical distances h and j of the two centers of mass, their longitudinal distance k and the wheel base $l + b$, i.e. the distance between the tire-road contact points P and S. The steering mechanism is characterized by the steering head angle ϵ and the normal trail t. Numerical values of parameters have been taken from a well established model [6] and are reported in Table 4 of Appendix B.

B. MOTORCYCLE'S RELATIVE COORDINATES

Relative coordinates define the position and orientation of motorcycle's bodies with respect to each other. The present paper considers the right-handed coordinate systems (CSs) shown in Fig. 1: Σ_0 is the inertial CS whose X_oY_o-plane represents the road surface with Z_o-axis pointing downwards; Σ_1 originates in A and rotates by the yaw angle ψ about Z_o-axis; Σ_2 originates in A and rotates by the roll angle ϕ about X_1-axis; a rotation of Σ_2 by the steering head angle ϵ about Y_2-axis and a translation to point B generates the CS Σ_3; a rotation of Σ_3 by an angle δ and a translation to G_f generates the CS Σ_4. The resulting kinematics chain has the following DoFs: the longitudinal and the lateral displacements of the moving point A in Σ_o, respectively x_o and y_o, vehicle's angular displacements ψ, ϕ, δ, respectively the yaw, the roll and the steering angle, the front and the rear wheels spinning θ_r, θ_f.

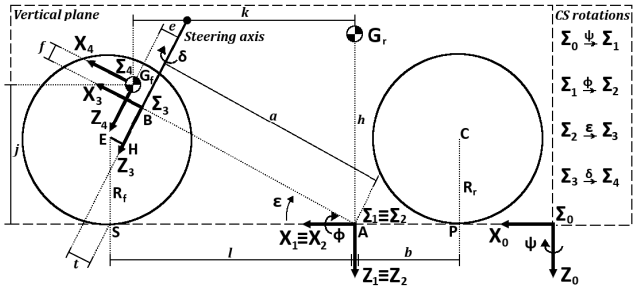

FIGURE 1. Motorcycle geometric parameters and reference frames.

C. MOTORCYCLE'S DYNAMICS

The dynamics of the AWD motorcycle is described by a set of 2^{nd} order nonlinear ordinary differential equations (ODEs) obtained by Euler-Lagrange's formalism (1), where the vector of the generalized coordinates is $\boldsymbol{q} = [x_1, y_1, \psi, \phi, \delta, \theta_r, \theta_f]^T$, and x_1, y_1 represent the displacements of the reference point A in the CS Σ_1. The term $T = T(\boldsymbol{q}, \dot{\boldsymbol{q}})$ is system's kinetic energy, $V = V(\boldsymbol{q})$ is the potential energy. Appendix A-A

will provide the derivation of T and V needed to solve (1), the results are summarised in (32), (37), (41), (42) and (50). The term $\boldsymbol{Q_q}$ is the vector of the generalized forces acting on the generalized coordinates.

$$\frac{d}{dt}\left(\frac{\partial T}{\partial \dot{\boldsymbol{q}}}\right) - \frac{\partial T}{\partial \boldsymbol{q}} + \frac{\partial V}{\partial \boldsymbol{q}} = \boldsymbol{Q_q} \tag{1}$$

The full actuation of AWD motorcycle is obtained by introducing in $\boldsymbol{Q_q}$ three system's inputs, i.e. the rear and the front engine torques τ_{w_r}, τ_{w_f}, respectively applied on the transverse axes of the rear and front wheel, and the torque τ applied on the handlebar by the rider. The vector $\boldsymbol{Q_q}$, can be defined as $\boldsymbol{Q_q} = [Q_{x_1}, Q_{y_1}, Q_\psi, Q_\phi, Q_\delta, Q_{\theta_r}, Q_{\theta_f}]^T$. It is composed of the forces and moments acting on the motorcycle's generalized coordinates $\boldsymbol{q}$. They mainly arise from the tire-road interaction and from the steering torque effects.

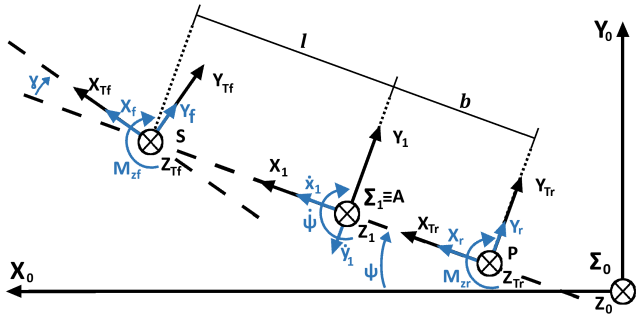

FIGURE 2. External tire forces, moments and their CSs.

In Fig. 2 are shown the external forces $X_i, Y_i, Z_i, i \in \{r, f\}$, acting on the tire-road contact points $P(i = r)$ and $S(i = f)$. Furthermore, P and S are the origins of the tires CSs $\Sigma_{Ti}(X_{Ti}, Y_{Ti}, Z_{Ti})$, $i \in \{r, f\}$ with respect to which the longitudinal and the lateral tire forces X_i, Y_i are defined. In the same CSs we assume Z_i as constant vertical loads. Referring to Fig. 2, the sum of the external forces along X_1 and Y_1 axes of the moving CS Σ_1, yields respectively the first two generalized forces Q_{x_1}, Q_{y_1}:

$$\begin{aligned} Q_{x1} &= X_f \cos\gamma - Y_f \sin\gamma + X_r \approx X_f + X_r \\ Q_{y1} &= Y_f \cos\gamma + X_f \sin\gamma + Y_r \approx Y_f + Y_r \end{aligned} \tag{2}$$

The approximations made in (2) hold under the assumption of small δ, which also implies small effective steering angle $\gamma = \delta\cos\epsilon$. Further detail about γ can be found in [33].

The third generalized force Q_ψ is the sum of the moments acting along Z_1-axis. It can be split into two contributes, Q_{ψ_1} and Q_{ψ_2}, as shown in (3). The first one includes the moments arising about Z_1-axis because of the external tire forces X_i, Y_i, $i \in \{r, f\}$ acting at distances b and l from point A. The second one includes the aligning moments $M_{z,i}$, $i \in \{r, f\}$, arising on the rear and the front tire contact patch [15]. The aligning moments will be derived later in section V-B devoted to the tire contact moments. Therefore, the term Q_ψ is:

$$\begin{aligned} Q_\psi &= \sum_{j=1}^{2} Q_{\psi_j} \\ &= (Y_f \cos\gamma + X_f \sin\gamma)l - Y_r\, b + (M_{z_f} + M_{z_r}) \\ &\approx Y_f\, l - Y_r\, b + (M_{z_f} + M_{z_r}) \end{aligned} \tag{3}$$

where the same approximation used in (2) holds. The fourth generalized force Q_ϕ is the sum of the moments about the X_1-axis, exerted by the tires external forces X_i, Y_i, Z_i and by the overturning moment M_{x_i} internally generated by the tire itself, being always $i \in \{r, f\}$. The external forces acting on the rear wheel do not contribute to this moment because of their null arm, therefore Q_ϕ is the sum of three contributes:

$$Q_\phi = \sum_{j=1}^{3} Q_{\phi_j} = -t\delta(Z_f \cos\phi - Y_f \sin\phi) + M_{x_r} + M_{x_f}\cos\gamma \tag{4}$$

The first term Q_{ϕ_1} is the X_1-component, linearized with $\sin\gamma = \gamma$ and $\cos\gamma = 1$, of the front external moment $\boldsymbol{M_{e_f}} = \boldsymbol{r_e} \wedge \boldsymbol{F_{e_f}}$ expressed in Σ_1. $\boldsymbol{F_{e_f}}$ is the front force with arm $\boldsymbol{r_e}$ (distance from the steering axis), both computed in Σ_1. Notice that in the front tire CS it is $\boldsymbol{F_{e_{f\,\Sigma_{Tf}}}} = [X_f, Y_f, Z_f]^T$ while in an auxiliary CS Σ_5 centered in S and oriented as Σ_4 is $\boldsymbol{r_{e\,\Sigma_5}} = [-t, 0, 0]^T$ hence these vectors converted to Σ_1 allow to compute $\boldsymbol{M_{e_f}}$. The terms Q_{ϕ_2} and Q_{ϕ_3} in (4) are respectively the components about X_1-axis of the overturning moments M_{x_r} and M_{x_f}, which will be derived in section V-B. The fifth generalized force Q_δ is the sum of the moments about the steering axis Z_3 of Fig. 1, which can be split into three contributes, Q_{δ_1}, Q_{δ_2} and Q_{δ_3}:

$$\begin{aligned} Q_\delta &= \sum_{j=1}^{3} Q_{\delta_j} \\ &= (\tau - K\dot{\delta}) + t\{[(Y_f \sin\phi - Z_f\cos\phi)\sin\epsilon \\ &\quad + (X_f - Y_f\gamma)\cos\epsilon]\delta - (Y_f\cos\phi + Z_f\sin\phi)\} \\ &\quad + M_{z_f}\cos\epsilon\cos\phi \end{aligned} \tag{5}$$

The first contribute includes the torque τ which is applied by the rider on the steering axis and the torque $-K\dot{\delta}$ due to the steering damper, where K is the damping constant. The contribute Q_{δ_2} includes the total moment acting along Z_3-axis, generated by the external tire forces X_f, Y_f, Z_f applied on the tire-road contact point S. It can be obtained by merely converting the moment $\boldsymbol{M_{e_f}}$ previously considered to the system Σ_4, and taking the third component, linearized with $\sin\gamma = \gamma$ and $\cos\gamma = 1$. The third component Q_{δ_3} is the aligning moment M_{z_f} along Z_3-axis. Finally, the last two generalized forces are related to the rear and front wheels and can be expressed as:

$$Q_{\theta_i} = -\tau_{w_i} + R_i X_i \quad i \in \{r, f\} \tag{6}$$

where $\tau_{w,i}$ are the engine torques applied on the rear and front wheels. The effects of the roll resisting moment are neglected since they are countered by wheel's traction. As can be seen, all the generalized forces depend on the longitudinal and the lateral tire forces X_i, Y_i, on the vertical load Z_i and on the

moments acting on the tires. The section V-B, devoted to the tire model, will explicit these forces and moments in terms of the kinematic variables of the vehicle.

IV. THE AWD SYMBOLIC MODEL: EQUATIONS OF MOTION

The seven EOMs representing the AWD motorcycle's dynamics are reported in this section. They have been obtained by applying to the nonlinear equations resulting from (1) a first order Taylor expansion around vehicle's vertical equilibrium point $\{\phi, \delta\} = \{0, 0\}$ and taking into account that $\gamma = \delta \cos\epsilon$. The first three nonlinear equations are relative to longitudinal, lateral and yaw motions and have been obtained by solving Lagrange's equations as follows [30], [34]:

$$\frac{d}{dt}\left(\frac{\partial T}{\partial \dot{x}_1}\right) - \frac{\partial T}{\partial \dot{y}_1}\dot{\psi} = Q_{x_1} \tag{7}$$

$$\frac{d}{dt}\left(\frac{\partial T}{\partial \dot{y}_1}\right) + \frac{\partial T}{\partial \dot{x}_1}\dot{\psi} = Q_{y_1} \tag{8}$$

$$\frac{d}{dt}\left(\frac{\partial T}{\partial \dot{\psi}}\right) - \frac{\partial T}{\partial \dot{x}_1}\dot{y}_1 + \frac{\partial T}{\partial \dot{y}_1}\dot{x_1} = Q_{\psi} \tag{9}$$

The remaining nonlinear equations relative to the motions of the roll, the steer and of the two wheels have been obtained by directly solving (1) with respect to the generalized coordinates $\phi, \delta, \theta_r, \theta_f$, whose generalized forces are, respectively, $Q_\phi, Q_\delta, Q_{\theta_r}, Q_{\theta_f}$. The following linearized EOMs have been found:

$$\begin{aligned}[\ddot{x}_1] \quad & (M_f + M_r)(\ddot{x}_1 - \dot{y}_1\dot{\psi}) - M_f k\dot{\psi}^2 - M_f e\cos\epsilon\dot{\delta}^2 \\ & - 2(M_r h + M_f j)\dot{\psi}\dot{\phi} - 2M_f e\dot{\delta}\dot{\psi} - X_r - X_f = 0\end{aligned} \tag{10}$$

$$\begin{aligned}[\ddot{y}_1] \quad & (M_f + M_r)(\ddot{y}_1 + \dot{x}_1\dot{\psi}) + (M_r h + M_f j)\ddot{\phi} \\ & + M_f e\ddot{\delta} + M_f k\ddot{\psi} - Y_r - Y_f = 0\end{aligned} \tag{11}$$

$$\begin{aligned}[\ddot{\psi}] \quad & M_f k\ddot{y}_1 + (M_f k^2 + I_{fz}\cos^2\epsilon + I_{fx}\sin^2\epsilon + I_{rz})\ddot{\psi} \\ & + \left[(I_{fz} - I_{fx})\cos\epsilon\sin\epsilon - C_{rxz} + M_f jk\right]\ddot{\phi} \\ & + (I_{fz}\cos\epsilon + M_f ek)\ddot{\delta} + (i_{fy} + i\beta_f)\dot{\theta}_f\dot{\phi} \\ & + (i_{ry} + i\beta_r)\dot{\theta}_r\dot{\phi} + (i_{fy} + i\beta_f)\sin\epsilon\dot{\theta}_f\dot{\delta} + M_f k\dot{x}_1\dot{\psi} \\ & + Y_r b - Y_f l - M_{z_r} - M_{z_f} = 0\end{aligned} \tag{12}$$

$$\begin{aligned}[\ddot{\phi}] \quad & (M_r h + M_f j)\ddot{y}_1 + [M_f jk + (I_{fz} - I_{fx})\cos\epsilon\sin\epsilon \\ & - C_{rxz})]\ddot{\psi} + (M_r h^2 + M_f j^2 + I_{rx} + I_{fx}\cos^2\epsilon \\ & + I_{fz}\sin^2\epsilon)\ddot{\phi} + (M_f ej + I_{fz}\sin\epsilon)\ddot{\delta} - (i_{ry} + \beta_r i)\dot{\theta}_r\dot{\psi} \\ & - (i_{fy} + \beta_f i)\dot{\theta}_f\dot{\psi} + (M_r h + M_f j)\dot{x}_1\dot{\psi} \\ & - (i_{fy} + \beta_f i)\cos\epsilon\dot{\theta}_f\dot{\delta} - (M_r h + M_f j)g\phi \\ & + (tZ_f - M_f eg)\delta - (I_{fy} + i\beta_f)\cos\epsilon\delta\ddot{\theta}_f \\ & - M_{x_r} - M_{x_f} = 0\end{aligned} \tag{13}$$

$$\begin{aligned}[\ddot{\delta}] \quad & M_f e\ddot{y}_1 + (M_f ek + I_{fz}\cos\epsilon)\ddot{\psi} + (M_f ej + I_{fz}\sin\epsilon)\ddot{\phi} \\ & + (M_f e^2 + I_{fz})\ddot{\delta} - (i_{fy} + i\beta_f)\sin\epsilon\dot{\theta}_f\dot{\psi} + M_f e\dot{x}_1\dot{\psi} \\ & + (i_{fy} + i\beta_f)\cos\epsilon\dot{\theta}_f\dot{\phi} + (tZ_f - M_f eg)\phi \\ & + (tZ_f - M_f eg)\sin\epsilon\delta + tX_f\cos\epsilon\delta + K\dot{\delta} - t\,Y_f \\ & - M_f e\cos\epsilon\delta\ddot{x}_1 - M_{z_f}\cos\epsilon = \tau\end{aligned} \tag{14}$$

$$[\ddot{\theta}_r] \quad (i_{ry} + i\beta_r^2)\ddot{\theta}_r + (i_{ry} + i\beta_r)\dot{\psi}\dot{\phi} = -\tau_{w_r} + R_r X_r \tag{15}$$

$$\begin{aligned}[\ddot{\theta}_f] \quad & (i_{fy} + i\beta_f^2)\ddot{\theta}_f + (i_{fy} + i\beta_f)\dot{\psi}\dot{\phi} - (i_{fy} + i\beta_f)\cos\epsilon\dot{\phi}\dot{\delta} \\ & + (i_{fy} + i\beta_f)\sin\epsilon\dot{\psi}\dot{\delta} = -\tau_{w_f} + R_f X_f\end{aligned} \tag{16}$$

where $k = a\cos\epsilon + e\cos\epsilon - f\sin\epsilon$ and $j = a\sin\epsilon + e\sin\epsilon + f\cos\epsilon$. Despite the tricky symbolism, due mainly to the full parametric representation of EOMs, the whole system is still described by the seven variables in $\boldsymbol{q}$. The only quantities still missing to be able to integrate the seven EOMs are the tire forces X_i, Y_i and the moments $M_{z_i}, M_{x_i}, i \in \{r, f\}$ which will be provided in the following section.

V. THE TIRE MODEL

An effective simulation of motorcycle dynamics requires a proper tire model able to describe most of phenomena arising from the tire-road interaction. This section is devoted to compute the longitudinal and lateral tires forces as well as the aligning and the overturning moments acting on the tires contact points. For this purpose, the widely accepted model conceived by Pacejka [15] has been adapted to the AWD symbolic model. Pacejka describes the tire forces and moments in terms of the so-called Magic Formula [15], which are functions of the tire slip. In Pacejka's model the axes systems are in accordance with the standard SAE J670 and 4976 (shown in Fig. 3a). In automotive, however, the ISO 8855 1991 (shown in Fig. 3b) is currently adopted as simulation-oriented standard for complex models. For this reason, the latter has been here adopted in order to easily compare the AWD symbolic model of the motorcycle with the model developed by means of a multibody software.

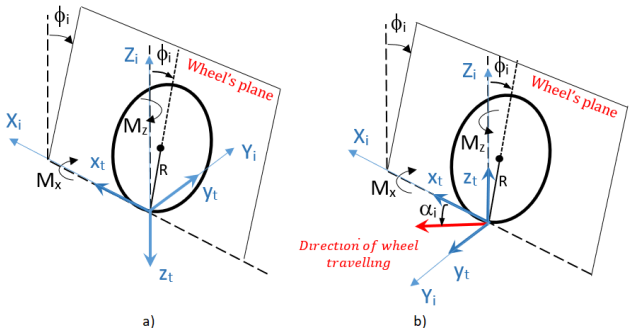

FIGURE 3. Tire external forces and internal moments: a) std SAE, b) std ISO.

The modeling of the tire forces and moments requires two essential wheel's kinematic quantities, the longitudinal slip λ and the side slip α [15]. Such quantities are defined as follow:

$$\lambda = -\frac{v_x - \omega R_e}{v_x} \qquad \alpha = \arctan\frac{v_y}{|v_x|} \tag{17}$$

where ω is the wheel's angular velocity, R_e is the effective rolling radius, v_x and v_y are the longitudinal and the lateral velocities of the tire-road contact point. Equation (17) is generally used by multibody software. As first analysis, the effective radius was simulated in both symbolic and multibody model by using the formulation defined by Pacejka.

Under the assumptions imposed on the motorcycle model, it can be shown that the deformation of the tire is negligible compared to the unloaded tire, as well as its effects. To further simplify the symbolic implementation, the effective radius R_e is replaced with the unloaded radius R_i, $i \in \{r, f\}$ while the multibody model keeps the standard definition (17). This choice simplifies the implementation without affecting the model accuracy as proven later by comparing the two models in simulation. In literature, the tire-road interaction has been described by two major models which differ in the way the longitudinal and lateral dynamics are coupled. The first one is the completely empirical model [15] which describes forces and moments by means of a set of Magic Formula, where the coupling effect is taken into account by multiplying the pure slip formulation of each dynamics with a proper weighting function. This implies the coupling is hidden in the formula. The second one is the semi-empirical model, it uses a subset of Magic Formula in pure slip condition which are function of the theoretical slip computed by the Brush model [15]. The majority of the multibody software use the former approach, however, the latter has been chosen in this paper coherently with its purpose of preserving the representation of the physical phenomena through a theoretical formulation, and have proved more suitable for the symbolic formulation. The Brush model considers the coupling effects by introducing three theoretical slip quantities, the theoretical longitudinal slip σ_{xi}, the theoretical lateral slip σ_{yi} and the total theoretical slip σ_i, defined as follows:

$$\begin{cases} \sigma_{xi} \triangleq \dfrac{\lambda_i}{1+\lambda_i} \\ \sigma_{yi} \triangleq \dfrac{\tan \alpha_i}{1+\lambda_i} \end{cases} \quad \sigma_i = \sqrt{\sigma_{xi}^2 + \sigma_{yi}^2} \quad i \in \{r, f\} \tag{18}$$

where λ_i and α_i are the slip quantities given in (17) specialized for the rear and the front wheel. These quantities are reported in Appendix A-B. The total theoretical slip σ_i is precisely the argument of the Magic Formula describing the contact forces and moments in the semi-empirical model, these are described in the following subsections.

A. TIRE CONTACT FORCES

The longitudinal and the lateral contact forces acting on the tires, respectively X_i and Y_i, are modeled as follows:

$$\begin{aligned} X_i &= \frac{\sigma_{xi}}{\sigma_i}\frac{Z_i}{Z_o} X_i^o(\sigma_i^*) \\ Y_i &= \frac{\sigma_{yi}}{\sigma_i}\frac{Z_i}{Z_o} Y_i^o(\sigma_i^*, \phi_i^*) \end{aligned} \quad \textit{with} \quad \begin{aligned} \sigma_i^* &= \frac{Z_o}{Z_i}\sigma_i \\ i &\in \{r, f\} \end{aligned} \tag{19}$$

where Z_i represents the constant vertical load acting on the front and rear tires while Z_o is the nominal wheel load [15]. The lateral contact force also includes the effect of the inclination of the tire by considering the tire camber angle ϕ_i^*, where $\phi_r^* = \phi$ and $\phi_f^* = \phi + \delta \sin \epsilon$. Each force in (19) is composed of the product of three terms: a coupling factor, a load factor and an empirical Magic Formula ($X_i^o(\sigma_i^*)$ and $Y_i^o(\sigma_i^*, \phi_i^*)$) describing the force in pure slip condition. These Magic Formula are defined as:

$$\begin{aligned} X_i^o(\sigma_i^*) = {} & D_{x_i} \sin\{C_{x,i} \arctan[\sigma_i^* B_{x_i} \\ & - E_{x_i}(\sigma_i^* B_{x_i} - \arctan(\sigma_i^* B_{x_i}))]\} \end{aligned} \tag{20}$$

$$\begin{aligned} Y_i^o(\sigma_i^*, \phi_i^*) = {} & D_{y_i} \sin\{C_{y_i} \arctan[\sigma_i^* B_{y_i} - E_{y_i}(\sigma_i^* B_{y_i} \\ & - \arctan(\sigma_i^* B_{y_i}))] + C_{\phi_i} \arctan[\phi_i^* B_{\phi_i} \\ & - E_{\phi_i}(\phi_i^* B_{\phi_i} - \arctan(\phi_i^* B_{\phi_i}))]\} \end{aligned} \tag{21}$$

The values of the parameters B_{x_i}, C_{x_i}, D_{x_i}, E_{x_i}, B_{y_i}, C_{y_i}, D_{y_i}, E_{y_i}, B_{ϕ_i}, C_{ϕ_i}, E_{ϕ_i} and Z_o used in this paper are reported in Table 5 of Appendix B. These parameters are described by H. B. Pacejka in his book, and are the same used by the Adams Software. In particular, it has been adopted Pacejka's PAC-Motorcycle library, named PAC-MC (120/70R17-Dry). In literature, such parameters are identified by means of specific test bench and software, based on empirical approach and data acquisition. A detailed description of the acquisition procedures is described in Pacejka's book.

B. TIRE CONTACT MOMENTS

This subsection describes the overturning and the aligning contact moments taken into account in the generalized forces (3), (4), (5) of the proposed symbolic model. The formulation of the overturning moment is based on [15] and [35], the main contributions taken into account are due to the lateral force and rolling effects, as shown below:

$$M_{x,i} = R_i Z_i (q_{sx3} \frac{Y_i}{Z_o} - q_{sx2}\phi) \quad i \in \{r, f\} \tag{22}$$

where Z_i, Y_i and Z_o have been defined above. The parameters q_{sx2} and q_{sx3} are taken from the multibody tire model, their meanings are explained in [35] and their values are reported in Table 5 of Appendix B; this formulation allows the proposed tire model to well approximate the multibody software model, however for a more in-deep treatment, the reader can refer to [15]. The aligning moment is composed of three terms, the first one depends on the lateral force effect, the second one is related to the longitudinal force effect, also known as the coupling term, and the last one is due to the residual aligning moment. The aligning moments have been expressed in compact form as follows [15]:

$$M_{z,i} = -t_{r_i} Y_i + X_i (R_i (s_{sz2} (\frac{Y_i}{Z_o}) + s_{sz3}\phi)) + M_{res,i} \tag{23}$$

As shown, the lateral effect is modulated by the terms t_{r_i}, also known in the literature as the pneumatic trail [15]. This trail is described by a specific Magic Formula which is a function of the theoretical side slip σ_{yi} and the total slip quantities σ_i as follows:

$$t_{r_i} = \frac{\sigma_{yi}}{\sigma_i}\frac{Z_i}{Z_o} t_{r_{Ro,i}} \tag{24}$$

$$\begin{aligned} t_{r_{Ro,i}} = {} & D_{t_i} \cos\{C_{t_i} \arctan[B_{t_i}\sigma_i^* - E_{t_i}(B_{t_i}\sigma_i^* \\ & - \arctan(B_{t_i}\sigma_i^*))]\} \cos(\sigma_{yi}) \end{aligned} \tag{25}$$

the values of the parameters D_{t_i}, B_{t_i}, C_{t_i} are reported in Table 5 of Appendix B. The second term of (23) is the coupling

effect due to the longitudinal force X_i. As done for the overturning moment (22), the formulation of the aligning moment has been slightly simplified compared to the Pacejka model [15], [35], i.e. only the lateral and the roll effects have been kept as well as the residual term $M_{res,i}$. The parameters s_{sz2} and s_{sz3} are equivalent to those used in the multibody tire model described in [35] and their values are reported in Table 5 of Appendix B. Referring to the residual aligning moment $M_{res,i}$, in order to compare its effect with the completely empirical model used by multibody tools, the formulation here proposed differs from the semi-empirical model that is known in the literature [15]. Such difference consists in the use of a Magic Formula depending on the theoretical slip σ_i^*, σ_{yi} of the Brush model. The Magic Formula is derived from the completely empirical model (see parameters in Table 5, Appendix B) and depends on the roll angle ϕ. A correction factor $(\sigma_{yi}/\sigma_i)(Z_i/Z_o)$ is introduced to take into account the side slip effect and vertical load normalization, therefore the formula reads as:

$$M_{res,i} = \frac{\sigma_{yi}}{\sigma_i}\frac{Z_i}{Z_o}M_{Ro,i} \tag{26}$$

$$M_{Ro,i} = D_{res_{\phi,i}}\cos(\arctan(B_{res_i}\sigma_i^*))\cos\sigma_{yi} \tag{27}$$

$$D_{res_{\phi,i}} = a_i\phi(b_i|\phi| + c_i) \tag{28}$$

VI. THE AWD MULTIBODY MODEL

Taking into account that in many high-tech fields such automotive, aerospace etc., the multibody analysis is a test-bench to simulate tests and behaviors of real prototypes during their development as a new product [4], the proposed model of this new kind of vehicle will be later compared with a higher-realistic multibody model which is here introduced. The MSC Adams software has been used to develop the AWD motorcycle in a multibody environment (Fig. 4). In order to have a test-bench as close as possible to the reality, the vertical dynamics has been included in the Adams model, thus, it includes both the front and rear wheel suspension in order to pursue the best fidelity. The Adams model uses the same linear dimensions, masses, inertia and tires model used in the symbolic model. Therefore, under the same input torques, suitably chosen in order to not trigger the vertical dynamics, it is expected a similar behavior of both symbolic and Adams models. In order to simulate the full dynamics of the AWD motorcycle in the multibody environment, at least a model consisting of four rigid bodies is required. This model has 11 DOFs for describing the bodies relative motion, 3 translational about the axes of the motorcycle CS (previously marked as Σ_1), 3 rotational (Roll, Pich, Yaw), 2 rotations about wheels revolution axes, 1 rotation about steering axis, 1 translational along the steering axis due to the front suspension system and 1 rotational about an axis parallel to Y_2-axis due to the rear suspension system. The road is locked by a fixed joint to the ground CS (previously marked as Σ_0). The rear frame of the motorcycle has been split into two rigid bodies: a rear frame without the wheel, including the rear engine, the propellant storage system, the saddle and the rider, and a second one representing the rear wheel. This has been done to allow the insertion of tire-road constraint in multibody environment. The same procedure has been performed for the front frame, by splitting the front wheel from the front frame. The position of the centers of mass and the inertia matrices of these new bodies have been suitably rearranged (see Table 6 of Appendix B for the multibody model parameters). As regards to the body joints, the front wheel is fixed to the suspension by a revolute joint which is fixed to the fork by a prismatic joint, the rear wheel is similar, but a second revolute joint at distance b from the wheel fixes the suspension to the rear frame; the front and rear frames are connected by a revolute joint about the steering axis. A steering damper is also modeled by a rotational spring damper acting between the two frames. The motorcycle is actuated by the torques applied to the revolute joints of both the wheels and to the steering mechanism. These torques will have the same profile of the control inputs of the AWD symbolic model. The MSC Adams tire model has been implemented to model the tire-road interaction. It uses the fully empirical tire model, based on [15] and it is illustrated in [35]. Note that in Adams the CS, defining tire forces and moments, is defined according to the standard ISO 8855, nevertheless the Adams tire model is equivalent to the one from Pacejka [15], which uses SAE standard, as previously shown in the tire section. In the multibody environment, additional CSs equivalent to those from the symbolic model (Σ_0, Σ_1, Σ_2, Σ_3, Σ_4) were defined, so that the generalized coordinates could be measured along the same axes in both models, this allowing to coherently compare such variables.

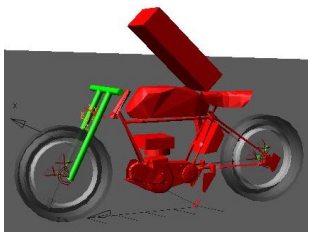

FIGURE 4. Multibody model of the AWD motorcycle.

VII. THEORETICAL AWD MODEL VERIFICATION

In order to validate the proposed AWD motorcycle model, a two steps procedure has been followed. This section concerns the first step and it provides the theoretical evaluation of the balance of forces and moments acting on the vehicle in steady turning, moreover the power balance is also verified. The next section will describe the second step of validation, where a comparison of the behavior of the AWD motorcycle model with the multibody software counterpart will be made. The first validation has followed the procedure described in [25]. The vehicle in steady turning has been simulated and the following three conditions have been verified in order to hold the vehicle in equilibrium:

- The sum of the external forces acting on the vehicle must equal the sum of the inertial and gravitational forces;
- The sums of the moments acting on the vehicle must equal zero;
- The power provided to the system by the motors must equal the power losses.

The steady state condition for the vehicle has been achieved by means of a simple rider model controlling the driving torque and the steering torque in order to have the motorcycle running along a circular trajectory with a radius of curvature of 200 m at a constant velocity of 15 m/s. In this state other kinematic parameters are: roll angle $\phi = 7.4$ deg, steering angle $\delta = 0.53$ deg; yaw velocity $\dot{\psi} = 0.075\, rad/s$. The rider model follows a well known schema, e.g. the one reported in [24] and it consists of two PI (Proportional Integrative) controllers with values $P_1 = 2, I_1 = 210, P_2 = 50, I_2 = 150$. In order to verify the first condition the following balance equation was considered that expresses the force error vector $\Delta \boldsymbol{F}$ as:

$$\Delta \boldsymbol{F} = \sum_i \boldsymbol{F}_{i,tire} + \sum_j M_j \left(\boldsymbol{\omega}_j \wedge \boldsymbol{v}_{G_j} + \boldsymbol{g}\right) + \boldsymbol{F}_{aero} \quad (29)$$

TABLE 1. Force balance - components.

Force	Description
$\boldsymbol{F}_{i,tire}$	External force vector on the ith tire $= [X_i, Y_i, Z_i]^T$
$M_j\,(\boldsymbol{\omega}_j \wedge \boldsymbol{v}_{G_j})$	Inertial force vector on the ith COM $\boldsymbol{\omega}_j$ =Rotational speed vector of the jth COM $\boldsymbol{v}_{G_j}$ =velocity vector of the jth COM
$M_j \boldsymbol{g}$	Gravitational force, with $\boldsymbol{g} = [0, 0, 9.81]^T$
$\boldsymbol{F}_{aero}$	Aerodynamic force vector with G_r as its center of pressure $\simeq \boldsymbol{F}_{drag} = [-0.5\rho_{air} C_D\, A\, v_f^2, 0, 0]^T$ $\rho_{air} = 1.167 Kg/m^3, (C_D\, A) = 0.7m^2$ v_f = longitudinal velocity of the vehicle

where the subscript $i \in \{r, f\}$ stands for the rear and the front tire/wheel, while the subscript $j \in \{r, f\}$ stands for the rear and the front center of mass (COM) having mass M_j. All the vectors of (29) are referred to the moving CS Σ_1 and their meaning are detailed in Table 1. In the term $\boldsymbol{F}_{aero}$ only the drag component is considered hence the lift force, the side force and their relative moments have been neglected. The importance of aerodynamic forces on the performance and stability of motorcycles at high speeds was demonstrated in [7] and pointed out in [5]. Generally, aerodynamic forces are not negligible, in particular they are relevant at high speeds. In our research, we refer to low accelerations and not high speeds, resulting in low wind yaw angles and minor crosswind effects, in that case much of aerodynamic effects are negligible excepting for drag force. This is supported by experimental data and theoretical assessment in [7]. It was also found that in these conditions the lift force coefficient was close to zero, therefore validating the assumptions made in this work. Above evaluations are also confirmed by numerical findings: aerodynamic side force is proportional to the sideslip angle and the side force aerodynamic coefficient. Since we deal with sideslip value of 0.02 rad and side force aerodynamic coefficient that approximates zero, the contribution of the aerodynamic side force is about 3% of the drag force. Besides, the computed side force is about 2% of the lateral force acting on the front tire-road contact point and 1% of the lateral force acting on the rear tire-road contact point. These results come from the evaluation of experimental data relating to a motorcycle running a curve at a constant speed of 15 m/s and different yaw angles. They seem to fully agree with the assumptions made.

In Fig. 5.a is depicted the behavior of the norm of the vector $|\Delta \boldsymbol{F}|$, which reaches a value of 0.4 N at steady state. Such quantity is 0,04% of the overall force acting on the vehicle in the steady state.

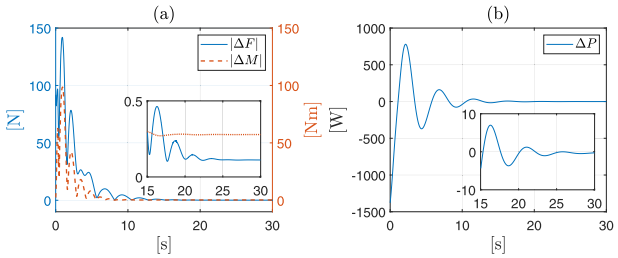

FIGURE 5. Fig (a): Time evolution of force and moment vectors' norm; zoomed graph: evolution in time frame 15 - 30 sec. Fig (b): Time evolution of resulting power; zoomed graph: evolution in time frame 15 - 30 sec.

In order to verify the second condition related to the moments balance, the following balance equation was considered that expresses the moment error $\Delta \boldsymbol{M}$ as:

$$\begin{aligned}\Delta \boldsymbol{M} &= \sum_i \boldsymbol{M}_{i,tire} + \sum_i \boldsymbol{M}_{i,tire_{int}} \\ &\quad + \sum_j (\boldsymbol{M}_{j,inertial} + \boldsymbol{M}_{j,grav}) + \sum_i \boldsymbol{M}_{i,gyro} + \boldsymbol{M}_{aero} \\ &= \sum_i (C_i - A)_{\Sigma_1} \wedge \boldsymbol{F}_{i,tire} + \sum_i \boldsymbol{M}_{i,tire_{int}} \\ &\quad + \sum_j (G_j - A) \wedge M_j (\boldsymbol{\omega}_j \wedge \boldsymbol{v}_{G_j} + \boldsymbol{g}) + \sum_i \boldsymbol{M}_{i,gyro} + \boldsymbol{M}_{aero}\end{aligned} \quad (30)$$

again, the subscripts i, j maintain the meaning defined above. The components of (30) are detailed in Table 2. In Fig. 5.a is depicted the trends of the norm vector $|\Delta \boldsymbol{M}|$, at steady state

TABLE 2. Moments balance - components.

Moments	Description
$\boldsymbol{M}_{i,tire}$	Moments on ith tire due to external forces $\boldsymbol{F}_{i,tire}$ and $(C_i - A)_{\Sigma_1}$ =arms vectors with $C_i \in \{P, S\}$
$\boldsymbol{M}_{i,tire_{int}}$	Aligning+overturning moments on the ith tire (sec V-B)
$\boldsymbol{M}_{j,inertial} + \boldsymbol{M}_{j,grav}$	Moments due to inertial and gravitational forces applied on $(G_j - A)_{\Sigma_1}$ = jth COM position
$\boldsymbol{M}_{i,gyro}$	Gyroscopic moment acting on the ith wheel $=\dot{\boldsymbol{H}}_{i,\Sigma_1} + \dot{\boldsymbol{\psi}} \wedge \boldsymbol{H}_{i,\Sigma_1} = \dot{\boldsymbol{\psi}} \wedge \boldsymbol{H}_{i,\Sigma_1}$ $\boldsymbol{H}_{i,\Sigma_1}$ =angular momentum ith wheel in Σ_1 $\dot{\boldsymbol{H}}_{i,\Sigma_1} = 0$ in steady-state,$\dot{\boldsymbol{\psi}} = [0, 0, \dot{\psi}]^T$
$\boldsymbol{M}_{aero}$	Yaw moment along Z_1-axis generated by $\boldsymbol{F}_{aero}$

is stable at 0.3 Nm, which is 0.06% of the resulting moments acting on the motorcycle. Finally, the third condition regarding the power balance has been verified by considering the power error ΔP, expressed as:

$$\Delta P = \sum_i P_{i,drive} + \sum_i P_{i,slip} + \sum_i P_{i,tire} + P_{aero} \quad (31)$$

where $i \in \{r, f\}$. Each component of (31) is detailed in Table 3. In Fig. 5.b is shown how the power checksum behave, and at steady state it reaches a mean value of 0.32 W between 15 and 25 seconds. Such value represents a 0.022% of the power provided by the traction system of 1446 W.

TABLE 3. Power balance - components.

Power	Description
$P_{i,drive}$	Power supplied to ith wheel by the motor= $\tau_{w_i}\,\dot{\theta}_i$
$P_{i,slip}$	Slip power losses ith tire=$X_i\,v_{sx_{Ti}} + Y_i\,v_{y_{Ti}}$ (tire CS Σ_{Ti})
	$v_{sx_{Ti}}, v_{y_{Ti}}$=long. and lateral slip velocities ith contact point
$P_{i,tire}$	Power loss due to aligning moment= $M_{z,i}\omega_i$
	$M_{z,i}$=align. moment (sec.V-B),ω_i=wheels angular speed along Z_1
P_{aero}	Aerodynamic power loss=$F_{drag}\dot{x}_1$, with $\dot{x}_1$ vehicle speed along X_1

VIII. COMPARATIVE VALIDATION AND RESULTS

In this section, the AWD motorcycle model will be further validated by means of comparative simulations with the multibody software counterpart. Furthermore, simulation tests highlighting AWD features pointed out by experienced riders will be provided. The proposed symbolic model has been implemented in Matlab Simulink environment. Comparative simulations, described in the next subsection, have investigated model reliability and effectiveness in two noteworthy conditions: maneuvers with roll and steering angles exceeding the linearization range; acceleration in cornering of AWD motorcycle when coupling dynamics is triggered. A further subsection will provide AWD vehicle behaviors compared with the rear-wheel-drive (RWD) vehicle.

A. CORNERING COMPARATIVE VALIDATION

Two simulations will be proposed here, named minor steering torque (mS) and major steering torque (MS). Both aims to estimate errors between symbolic and multibody models by comparing the roll angle, the steering angle and the trajectories. Before detailing simulation results, it is worth noting that the comparison was made with a higher-realistic multibody model than the symbolic one. Adams model includes vertical dynamics, more degrees of freedom, is free of linear approximations, and uses Adams tire model. For our purposes, it is closest to a real AWD byke.

Fig. 6 shows the wheels input torques applied in both simulations, that are: τ_{w_r}, τ_{w_f} the rear and front respectively; the steering torques named τ_{mS}, τ_{MS} are respectively used in mS and MS simulations. A ratio of $\tau_{MS} = 3\tau_{mS}$ will be considered. In order to avoid the overlapping of torques transients, wheels torques act after the steering torques transient, at $t = 10$s. These inputs have been generated in Adams

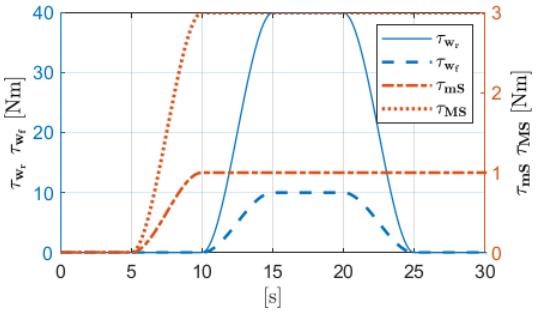

FIGURE 6. Rear and front wheel's torques (τ_{wr}, τ_{wf}) and minor and major steering torques (τ_{mS}, τ_{MS}).

software and exported to Matlab in order to have the same input profiles for both models.

As the multibody model has both vertical and suspension dynamics, it is possible to quantify the fore-and-aft load transfer under the acceleration generated by the torque applied in Fig. 6. As shown in Fig. 7, the rear and front vertical forces F_{z_r}, F_{z_f} have a load transfer of about 70 N from the front to the rear frames. This clearly means a negligible force compared with the total load of the vehicle of 2433.8 N, about 3%. It was tested that is acceptable to neglect such effects even at 10% of load transfer, as the two models still show compatible simulation results.

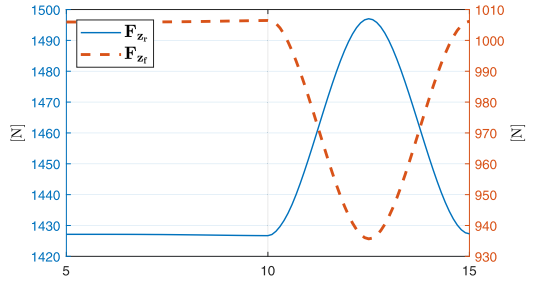

FIGURE 7. Trend of rear and front vertical forces (F_{z_r}, F_{z_f}) under moderate vehicle acceleration.

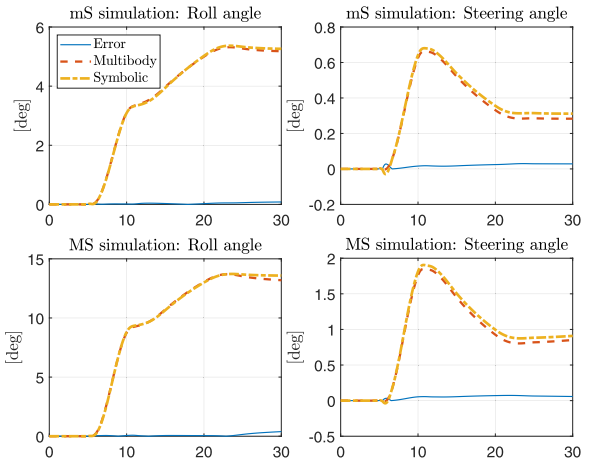

FIGURE 8. AWD models: comparisons of roll and steering angles.

Fig. 8 shows the comparison between the responses of AWD symbolic model versus AWD multibody model for

the two simulations scenarios. In *mS* scenario the roll angle reaches 5.5 *deg* while the steering angle remains limited to 1 degree. The roll error magnitude between the two models remains below 2%, confirming expected results under linearization assumptions. In the *MS* scenario larger steering torque is applied, causing the vehicle to roll up to 14 *deg* and to steer up to more than 2 *deg*, nevertheless the roll error remains limited under 8%. On the other hand, the different steering angle behaviors (Fig. 8) produce a trajectory error between the two models as shown in Fig. 9. In the first 10 seconds the trajectory error is minimal, afterwards the difference is stressed during the activation of the wheels torque. As an overall result, the effect of the steering error on the trajectory appears negligible and the symbolic model performs the same as the multibody model both under the assumptions made of small angles and beyond them. Similar overperformance in the roll angle was outlined in a previous work [36] related to single track vehicle.

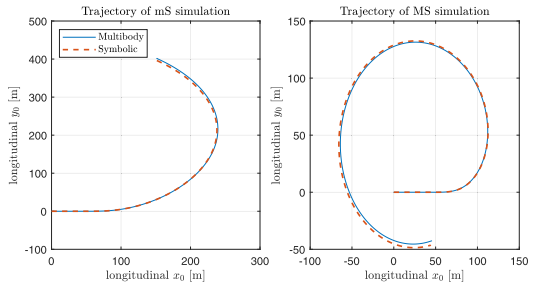

FIGURE 9. AWD models: trajectories comparisons.

B. AWD TESTING RESULTS

Specific simulations have been carried out in order to highlight the effects of the front wheel drive on motorcycle's dynamics. Two relevant driving scenarios named d_1 (entering the curve) and d_2 (exiting the curve) are here considered. The same steering torque τ_s, shown in Fig. 10, is used in both scenarios. In d_1, the motorcycle is accelerated by τ_{d_1} when approaching a curve, namely between 5 and 11 seconds when the steering torque is increasing. In scenario d_2 the vehicle is accelerated by τ_{d_2} when coming out of the curve, namely between 11 and 17 seconds. The simulations start with the motorcycle in vertical trim and constant speed of 8 m/s. For each scenario, two simulations named RWD (Rear Wheel Drive) and AWD are carried out by considering two different driving torque distribution: in RWD the whole driving torque is applied to the rear wheel (as in a standard motorcycle); in simulation AWD the 20% of the driving torque is applied to the rear wheel and 80% to the front wheel. Fig. 11 shows the comparisons between the roll angle and yaw speed obtained in both simulations RWD and AWD for scenario d_1. As experienced by most riders, the RWD simulation shows that the use of a rear torque while approaching the curve is not advisable, because it affects the roll angle and yaw speed negatively, indeed the rear tire contact forces keep the vehicle

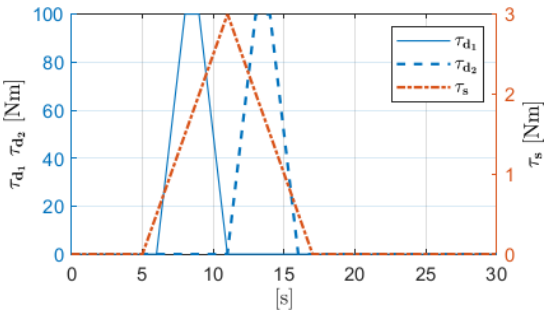

FIGURE 10. Steering torque τ_s applied in both scenarios d_1, d_2, while driving torque τ_{d_1} applied in d_1 and τ_{d_2} applied in d_2.

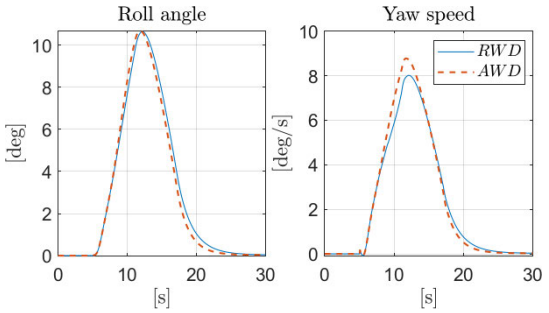

FIGURE 11. Scenario d_1 (entering the curve): roll angle and yaw speed comparison between RWD and AWD.

in vertical trim, countering the desired turning, such behavior resembles the oversteer effect. On the other hand, the AWD simulation shows that the use of the front torque in the same circumstances is even desirable to obtain a sharper cornering trajectory, in fact yaw speed reaches a higher peak value than that delivered by RWD. The same behavior affects the roll angle. This phenomenon resembles an understeer effect.

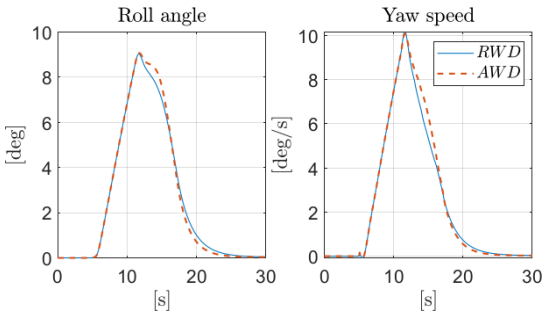

FIGURE 12. Scenario d_2 (exiting the curve): roll angle and yaw speed comparison between RWD and AWD.

In scenario d_2, when the front torque is acting (see Fig. 12 at $t = 11$ s), AWD yaw speed decreases slower with respect to the RWD case, as well as the roll angle is held around the maximum value. Here the front torque affects the behavior negatively while the rear torque, as expected, slightly affects the yaw speed as it appears steeper than the rising part of the trajectory ($t = [5; 11]$ s). This phenomenon resembles the behavior experienced by the few AWD riders. As they described, it's harder to regain the vertical trim while exiting

a curve by operating the front torque. To conclude, the simulations have shown that the use of a front drive eases the maneuver when approaching a curve, while it may interfere the coming out of a curve.

C. AWD HANDLING RESULTS

The front traction effect on motorcycle's handling can be considered advantageous or disadvantageous depending on the rider's intention. Indeed, if the rider accelerates with the front torque when approaching a cornering maneuver, a positive effect can be experienced facilitating the rider in the maneuver. On the contrary, the effect is negative if the front torque acts at the end of the curve, because more effort is required to the rider to restore the vehicle's vertical trim. In this subsection, the vehicle's handling is analyzed in various simulation tests characterized by a different value of the ratio between the steer and the roll angle. A feedback control action ensures the vehicle to have the same longitudinal speed along the trajectory. This control action guarantees that the motorcycle dynamics generated by different traction ratios is easily comparable, since it is clearly dependent by the longitudinal speed [6]. In the simulations, different traction distribution between rear and front wheels are tested in two different moments of the same cornering maneuver. The steer torque acts in all simulations from 5 to 17 seconds with the same trajectory shown in Fig. 10. The traction torque is generated by the feedback controller, which imposes the desired longitudinal speed from 8 m/s to 12 m/s. Such speed variation takes place in entering the curve from 5 to 11 seconds, while at the end of the cornering it occurs from 11 to 16 seconds. In all situations, the yaw rate differences are small (see Fig. 13 and 14), nonetheless, a higher value is reached when the front torque acts at the beginning of the cornering maneuver.

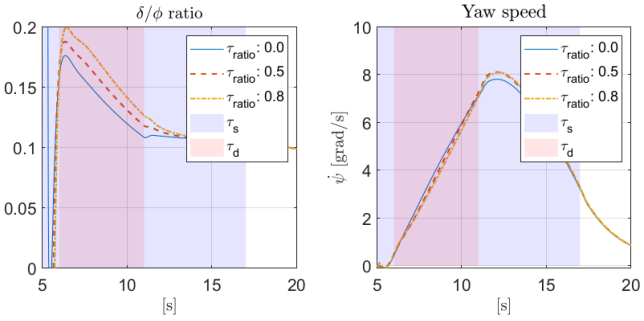

FIGURE 13. Entering the curve: steer/roll ratio and yaw speed comparison.

The effect of the front traction can be explained analyzing the ratio between steer and roll angle in Fig. 13. When the front torque is acting, this ratio is higher, which means that lower rolling angle can be achieved with the higher steering angle. This can be considered as a positive or negative effect depending on the intention of the rider. The Fig. 13 and 14 show three simulations with the following values of the rear-on-front torque ratio respectively: 0, indicating that only rear torque applied, 0.5, i.e., half torque is applied to the rear

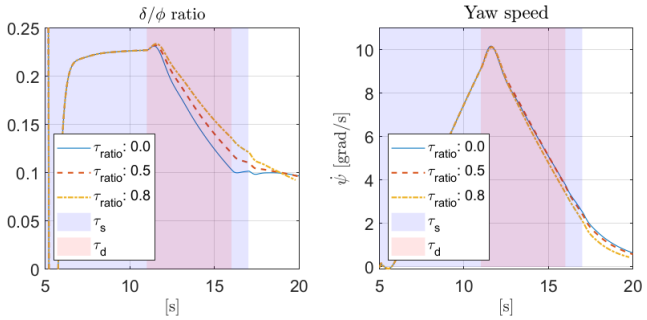

FIGURE 14. Exiting the curve: steer/roll ratio and yaw speed comparison.

wheel and half to the front one, 0.8, indicating 80% of the torque on the front wheel and 20% on the rear one. The time period when the steer torque acts is indicated by the blue area, while the red area shows the traction action period. When approaching the cornering maneuver at 7 seconds the ratio in Fig. 13 has a value of 0.2, while it is 0.17 when only the rear torque is acting. In other words, the steering angle can be higher with the same rolling angle and hence a smaller curvature radius can be achieved, if required by the rider. Conversely, in the scenario of Fig. 14, the front traction acts when the curve ends, and the effects lead to similar consideration as the ratio is higher. The reason to consider this last behavior as negative is based on the rider intention to end the curve by reaching the vehicle's vertical trim. If the rider aims at reaching such trim with a straight steer, this requires more effort when the front torque acts. Because of the higher rolling angle reached halfway in the cornering maneuver and the front torque action increasing the ratio δ/ϕ, the steer angle is delayed to reach the zero roll angle. If the rider's goal is to force the steer angle to reach faster the zero trim as intended, this will require more effort to the rider. By concluding, a handling ratio is introduced to better understand the effect of the front torque, and such effect proves to be bivalent as it eases the rider in approaching the cornering maneuver, whilst it hinders the rider when exiting a curve.

IX. CONCLUSIONS AND FUTURE WORKS

In this work, an AWD motorcycle model has been outlined and the relevant steps needed to derive the EOMs, linearized with respect to the roll and the steering angle have been shown. The model has been integrated with an adapted version, but nonetheless effective, of the tire model developed by H. B. Pacejka which describes, by means of a semi-empirical approach, the coupling between forces and moments arising on the tire-road contact points. The AWD motorcycle model thus obtained has been validated in two steps; the first one follows a theoretical approach commonly used in literature and it proves the modeled vehicle can be driven to an equilibrium condition. This is done by evaluating the balance of forces and moments acting on the vehicle in a steady state cornering maneuver; in the second step the AWD model

has been compared in simulations against a richer model of the same motorcycle, implemented in a multibody software. The comparison in cornering condition of the two models have shown small differences. Finally, further simulations have been carried out to evaluate the effects of a torque distribution on the vehicle dynamics. For this purpose an appropriate handling ratio has been proposed. The benefits and disadvantages of using full rear drive or AWD with torque distribution have been highlighted and the results agree with factual behaviors of an AWD motorcycle experienced by riders. Future works will aim to investigate more in-depth the best way to use the front traction in different scenarios, even when slip conditions occur; this will be functional to the developing of control systems that will properly act on the torque distribution in order to obtain improved and safer vehicle's behaviors without obstructing the driver.

APPENDIX A
KINEMATIC MODEL
A. KINETIC AND POTENTIAL ENERGIES

In this appendix the kinetic energy T and the potential energy V of the system are derived.

$$T = T_r + T_f + T_\omega \tag{32}$$

T_r and T_f are the kinetic energies of the rear and the front frame, they are given by:

$$T_i = \frac{1}{2} M_i \boldsymbol{v_i}^2 + \frac{1}{2} \boldsymbol{\omega_i}^T I_i \boldsymbol{\omega_i} \quad i \in \{r, f\} \tag{33}$$

where M_i, $\boldsymbol{I_i}$, are the inertial properties of the two frames, i.e. their masses and their inertia matrices respectively, $\boldsymbol{v_i}$ and $\boldsymbol{\omega_i}$ relate to the kinematic properties of the centers of mass G_i and represent the square of their speed vector and their angular velocity vector, respectively. The term T_ω takes into account the rotational extra terms not included in T_i such as the rotations of the wheels and flywheels.

The kinetic energy of the rear frame T_r, given by (33), depends on the speed $\boldsymbol{v_r}$ of the rear mass center G_r and on its angular velocity $\boldsymbol{\omega_r}$. The vector $\boldsymbol{v_r}$ is given by:

$$\boldsymbol{v_r} = \boldsymbol{v_A} + \boldsymbol{\omega_A} \wedge (G_r - A) = \begin{bmatrix} \dot{x}_1 - h \sin\phi\dot{\psi} \\ \dot{y}_1 + h\cos\phi\dot{\phi} \\ h \sin\phi\dot{\phi} \end{bmatrix} \tag{34}$$

where $\boldsymbol{v_A}$ and $\boldsymbol{\omega_A}$ are the speed and the angular velocity of Σ_1. The vector $\boldsymbol{\omega_r}$ is the angular velocity of Σ_2 and holds:

$$\boldsymbol{\omega_r} = \left[\dot{\phi},\ \sin\phi\dot{\psi},\ \cos\phi\dot{\psi}\right]^T \tag{35}$$

We assume I_r as the matrix of inertia of the rear frame whose inertia moments and inertia products are about axis parallel to $X_2Y_2Z_2$ through rear mass center. Their values are reported in Table 4 of Appendix B:

$$I_r = \begin{bmatrix} I_{rx} & 0 & -C_{rxz} \\ 0 & I_{ry} & 0 \\ -C_{rxz} & 0 & I_{rz} \end{bmatrix} \tag{36}$$

By substituting (34), (35) and (36) in (33), the rear kinetic energy becomes:

$$\begin{aligned} T_r = {} & \frac{1}{2} M_r[(\dot{x}_1 - h\sin\phi\dot{\psi})^2 + (\dot{y}_1 + h\cos\phi\dot{\phi})^2 \\ & + (h\sin\phi\dot{\phi})^2] + \frac{1}{2} I_{rx}\dot{\phi}^2 + \frac{1}{2} I_{ry}(\sin\phi\dot{\psi})^2 \\ & + I_{rz}(\cos\phi\dot{\psi})^2 - C_{rxz}\cos\phi\dot{\phi}\dot{\psi} \end{aligned} \tag{37}$$

The kinetic energy of the front frame T_f depends on the velocity $\boldsymbol{v_f}$ of G_f and its angular velocity $\boldsymbol{\omega_f}$. Therefore, by considering the speed $\boldsymbol{v_B}$ of the point B and its angular velocity $\boldsymbol{\omega_B}$, the velocity $\boldsymbol{v_f}$ is given by:

$$\begin{aligned} \boldsymbol{v_f} = {} & \boldsymbol{v_B} + \boldsymbol{\omega_B} \wedge (G_f - B) \\ = {} & \begin{bmatrix} \dot{x}_1 - \dot{\psi}(\sin\epsilon\sin\phi(a + e\cos\delta) + \\ + e\cos\phi\sin\delta + f\cos\epsilon\sin\phi) - \dot{\delta}e\cos\epsilon\sin\delta \\ \dot{y}_1 + \dot{\psi}(\cos\epsilon(a + e\cos\delta) - f\sin\epsilon) + \\ + \dot{\phi}\cos\phi\sin\epsilon(a + e\cos\delta) + \dot{\delta}e\cos\delta\cos\phi + \\ + \dot{\phi}f\cos\epsilon\cos\phi - \dot{\phi}e\sin\delta\sin\phi + \\ - \dot{\delta}e\sin\delta\sin\epsilon\sin\phi \\ \sin\phi\dot{\phi}\sin\epsilon(a + e\cos\delta) + \\ + \dot{\delta}e\cos\delta\sin\phi + \dot{\phi}e\cos\phi\sin\delta + \\ + \dot{\phi}f\cos\epsilon\sin\phi + \dot{\delta}e\cos\phi\sin\delta\sin\epsilon \end{bmatrix} \end{aligned} \tag{38}$$

The angular velocity $\boldsymbol{\omega_f}$ of G_f is the angular velocity of Σ_4 and it is given by:

$$\boldsymbol{\omega_f} = \begin{bmatrix} \dot{\psi}(\sin\delta\sin\phi - \cos\delta\cos\phi\sin\epsilon) + \dot{\phi}\cos\delta\cos\epsilon \\ \dot{\psi}(\cos\delta\sin\phi + \cos\phi\sin\delta\sin\epsilon) - \dot{\phi}\cos\epsilon\sin\delta \\ \dot{\delta} + \dot{\phi}\sin\epsilon + \dot{\psi}\cos\epsilon\cos\phi \end{bmatrix} \tag{39}$$

The inertia matrix I_f of the front frame, related to the principal axes of inertia $X_4Y_4Z_4$ is given by:

$$I_f = diag\left[I_{fx},\ I_{fy},\ I_{fz}\right] \tag{40}$$

The elements of I_f are reported in Table 4 of Appendix B. By using the quantities (38), (39) and (40) the front kinetic energy T_f becomes:

$$\begin{aligned} T_f = {} & \frac{1}{2} M_f[(\dot{x}_1 - e\cos\epsilon\sin\delta\dot{\delta} - (a\sin\epsilon\sin\phi + e\sin\delta\cos\phi \\ & + e\sin\epsilon\cos\delta\sin\phi + f\cos\epsilon\sin\phi)\dot{\psi})^2 \\ & + (\dot{y}_1 + a\sin\epsilon\cos\phi\dot{\phi} - e\sin\delta\sin\phi\dot{\phi} + e\cos\delta\cos\phi\dot{\delta} \\ & + e\sin\epsilon\cos\delta\cos\phi\dot{\phi} - e\sin\epsilon\sin\delta\sin\phi\dot{\delta} \\ & + f\cos\epsilon\cos\phi\dot{\phi} + (a\cos\epsilon + e\cos\delta\cos\epsilon - f\sin\epsilon)\dot{\psi})^2 \\ & + (a\sin\epsilon\sin\phi\dot{\phi} + e\sin\delta\cos\phi\dot{\phi} + e\cos\delta\sin\phi\dot{\delta} \\ & + e\sin\epsilon\cos\delta\sin\phi\dot{\phi} + e\sin\epsilon\sin\delta\cos\phi\dot{\delta} \\ & + f\cos\epsilon\sin\phi\dot{\phi})^2] + \frac{1}{2} I_{fx}[(\cos\epsilon\cos\delta\dot{\phi} + \sin\delta\sin\phi \\ & - \sin\epsilon\cos\delta\cos\phi)\dot{\psi}]^2 + \frac{1}{2} I_{fy}[-\cos\epsilon\sin\delta\dot{\phi} \\ & + (\cos\delta\sin\phi + \sin\epsilon\sin\delta\cos\phi)\dot{\psi}]^2 \\ & + \frac{1}{2} I_{fz}[\dot{\delta} + \sin\epsilon\dot{\phi} + \cos\epsilon\cos\phi\dot{\psi}]^2 \end{aligned} \tag{41}$$

In order to compute the total kinetic energy of the system (32) the extra kinetic energy T_ω must be derived. The contribute T_ω is related to the rotation of the wheels and the engine flywheels, it can be expressed by:

$$T_\omega = \sum_i T_{\omega_{w_i}} + \sum_i T_{fly_i} \quad i \in \{r, f\} \tag{42}$$

The terms $T_{\omega_{w_i}}$ are the kinetic energies of the rear and front wheel not taken into account by T_r and T_f, whereas T_{fly_i} are the rotational energies of the engines flywheels included in the vehicle. The contribute $T_{\omega_{w_i}}$ can be derived by defining $\boldsymbol{\omega}_{T_{w_i}}$ as the total angular velocity of the wheel, expressed as:

$$\boldsymbol{\omega}_{T_{w_i}} = \boldsymbol{\omega_i} + [0, \dot{\theta}_i, 0]^T \quad i \in \{r, f\} \tag{43}$$

where $\boldsymbol{\omega_i}$ was defined in (35) for $i = r$ and in (39) for $i = f$. The vector $[0, \dot{\theta}_i, 0]^T$ is the rotational angular velocity of the wheel, it is defined in Σ_2 for $i = r$ and in Σ_4 for $i = f$. The contribute $T_{\omega_{w_i}}$ can be derived as a difference of kinetic energies generated by $\boldsymbol{\omega}_{T_{w_i}}$ and $\boldsymbol{\omega_i}$ which yields:

$$T_{\omega_{w_i}} = \frac{1}{2}\boldsymbol{\omega}_{T_{w_i}}^T\, i_i\, \boldsymbol{\omega}_{T_{w_i}} - \frac{1}{2}\boldsymbol{\omega_i}^T\, i_i\, \boldsymbol{\omega_i} \quad i \in \{r, f\} \tag{44}$$

where i_i is the diagonal matrix of inertia of the wheel completely defined by the polar moment of inertia i_{r_y} and the camber inertia $i_{r_x} = i_{r_z}$, whose values are reported in Table 4 of Appendix B. Finally, by solving (44) for the rear and front wheels it yields:

$$T_{\omega_{wr}} = i_{ry}(\sin\phi\dot{\psi}\dot{\theta}_r + \frac{1}{2}\dot{\theta_r}^2) \tag{45}$$

$$T_{\omega_{wf}} = i_{fy}[(-\cos\epsilon\sin\delta\dot{\phi} + (\cos\delta\sin\phi + \sin\epsilon\sin\delta\cos\phi)\dot{\psi})\dot{\theta}_f + \frac{1}{2}\dot{\theta}_f^2] \tag{46}$$

Similarly, the engine flywheels contribute T_{fly_i}, $i \in \{r, f\}$, is derived by applying (44) and taking care to replace $T_{\omega_{w_i}}$ with T_{fly_i}, i_i with i_{fly_i} and $\boldsymbol{\omega}_{T_{w_i}}$ with $\boldsymbol{\omega}_{T_{fly_i}}$, the latter defined as:

$$\boldsymbol{\omega}_{T_{fly_i}} = \boldsymbol{\omega_i} + [0, \beta_i\dot{\theta}_i, 0]^T \quad i \in \{r, f\} \tag{47}$$

where β_i is the gear ratio between the wheel and the engine flywheel and i_{fly_i} is the polar moment of inertia of the flywheel. Therefore the kinetic energies of the flywheels hold:

$$T_{fly_r} = i_{fly_{r_y}}(\beta_r\sin\phi\dot{\psi}\dot{\theta}_r + \frac{1}{2}\beta_r^2\dot{\theta_r}^2) \tag{48}$$

$$T_{fly_f} = i_{fly_{f_y}}(-\cos\epsilon\sin\delta\beta_f\dot{\theta}_f\dot{\phi} + \cos\delta\sin\phi\beta_f\dot{\theta}_f\dot{\psi} + \cos\phi\sin\delta\sin\epsilon\beta_f\dot{\theta}_f\dot{\psi} + \frac{1}{2}\beta_f^2\dot{\theta}_f^2) \tag{49}$$

The values of the polar moments $i_{fly_{r_y}}$ and $i_{fly_{f_y}}$ are reported in Table 4 of Appendix B.

The potential energy of the system is the sum of the potential energy of two mass centers G_r and G_f and it is given by

$$V = \sum_i V_i = \sum_i M_i\, g\, z_i = M_r\, g\, z_r + M_f\, g\, z_f = M_r g h\cos\phi + M_f g(a\sin\epsilon\cos\phi - e\sin\phi\sin\delta + e\sin\epsilon\cos\delta\cos\phi + f\cos\epsilon\cos\epsilon) \quad i = \{r, f\} \tag{50}$$

TABLE 4. Symbolic model - geometric and inertial parameters.

parameter	notation	value	u.m. (SI)
M_f	mass of front frame	30.6472	kg
M_r	mass of rear frame	217.4492	kg
Z_f	front vertical force	-1005.3	N
Z_r	rear vertical force	-1428.5	N
I_{rx}	rear frame inertia x axis	31.184	kg m^2
I_{rz}	rear frame inertia z axis	21.069	kg m^2
C_{rxz}	product of inertia xz	1.7354	kg m^2
I_{fx}	front frame inertia x axis	1.2338	kg m^2
I_{fy}	front frame inertia y axis	0.835	kg m^2
I_{fz}	front frame inertia z axis	0.442	kg m^2
$i_{fy} = i_{ry}$	front and rear wheel inertia	0.7186	kg m^2
$i_{fly_{r_y}} = i_{fly_{f_y}}$	front and rear flywheel polar inertia	0.332	kg m^2
ϵ	caster angle	0.4715	rad
a	A-B distance	0.9485	m
b	A-P distance	0.4798	m
e	G_f-Z_3 (steering axis) distance	0.024384	m
f	z position of G_f	0.028347	m
h	G_r-A distance	0.6157	m
l	A-S distance	0.8346	m
R_r	rear wheel radius	0.3048	m
R_f	front wheel radius	0.3048	m
t	mechanical trail	0.11582	m
K	steering damper	6.78	$\frac{\text{N m}}{\text{rad s}}$

TABLE 5. Tire parameters.

•	Longitudinal	Lateral	Lateral ϕ^*	Aligning
Stiffness factor	B_{x_r}=8.189 B_{x_f}=7.0273	B_{y_r}=8.189 B_{y_f}=7.0273	B_{ϕ_r}=-0.5 B_{ϕ_f}=-0.493	B_{t_r}=5.141 B_{t_f}=5.172
Shape factor	C_{x_r}=1.612 C_{x_f}=1.612	C_{y_r}=1.197 C_{y_f}=1.197	C_{ϕ_r}=0.507 C_{ϕ_f}=0.507	C_{t_r}=1.711 C_{t_f}=1.711
Peak value	D_{x_r}=2012.3 D_{x_f}=1452.1	D_{y_r}=2195.7 D_{y_f}=1546.3	-	D_{t_r}=0.020 D_{t_f}=0.015
Curvature factor	E_{x_r}=-0.082 E_{x_f}=-0.348	E_{y_f}=E_{y_r}= $0.566\sin\sigma_r$ $+0.360$	E_{ϕ_f}=-22.497 E_{ϕ_r}=-22.497	-
Parameters				
Overturning	q_{sx2}=0.1252	q_{sx3}=0.0577	•	•
Aligning	s_{sz2}=0.022067	s_{sz3}=0.14968	•	•
Residual	a_r=-435.4 a_f=-306.41	b_r=0.029 b_f=0.046	c_r=0.069 c_f=0.0453	B_{res_r}=8.430 B_{res_f}=8.430
Nominal wheel load Z_o=1375				

where V_i is the potential energy of the mass center G_i, M_i is the mass of the frame i, g is the gravitational acceleration and z_i is the height of G_i with respect to the ground level. The terms z_i are easily derived by considering the component along Z_1 axis of the vector $(G_i - A)$ computed in Σ_1.

B. REAR AND FRONT SLIP

The rear and front lateral slip α_r and α_f are formulated as follows [15]:

$$\alpha_r = -\frac{\dot{y}_1 - b\dot{\psi}}{\dot{x}_1} \quad \alpha_f = \delta\cos\epsilon - \frac{\dot{y}_1 + l\dot{\psi} - t\dot{\delta}}{\dot{x}_1} \tag{51}$$

The longitudinal slip λ_r and λ_f are given by [15], [30]:

$$\lambda_i = -\frac{\dot{x}_1 + R_i\dot{\theta}_i - R_i\sin\phi\dot{\psi}}{\dot{x}_1} \quad i \in \{r, f\} \tag{52}$$

Considering the front wheel contact point S, the front longitudinal slip $\lambda_{i=f}$ is approximated by putting $\delta = 0$.

Equation (52) with $i = f$ fixes the error appearing in [30].

TABLE 6. Multibody model - geometric and inertial parameters.

•	Rear Frame	Front Frame	Rear Wheel	Front Wheel
Mass [kg]	201.9793	15.1773	15.469	15.469
CoM * [m]	$x = 0.0367$ $z = -0.6395$	$x = 0.7716$ $z = -0.6327$	$x = -0.479$ $z = -0.3048$	$x = 0.934$ $z = -0.3048$
Inertia ** [kg m^2]	$i_x = 29.214$ $i_y = 19.6319$ $i_z = 16.8753$ $C_{xz} = 3.8663$	$i_x = 0.5491$ $i_y = 0.1291$ $i_z = 0.4165$ $C_{xz} = 0.2429$	$i_x = 0.36$ $i_y = 0.718+\beta\,0.332$ $i_z = 0.36$ $C_{xz} = 0$ $\beta = 1$	$i_x = 0.36$ $i_y = 0.718+\beta\,0.332$ $i_z = 0.36$ $C_{xz} = 0$ $\beta = 0$
Suspension System				
Front suspension	K_f=12800 [$\frac{\mathrm{N}}{\mathrm{m}}$]	D_f=1000 [$\frac{\mathrm{N\,s}}{\mathrm{m}}$]		
Rear suspension	K_r=7753 [$\frac{\mathrm{N\,m}}{\mathrm{rad}}$]	D_r=100 [$\frac{\mathrm{N\,m\,s}}{\mathrm{rad}}$]		

* The Centre of Mass positions are defined in CS Σ_1 or point A with SAE standard, the Y axis position is always zero.

** The inertia matrices have the form: $I_i = \begin{bmatrix} i_x & 0 & -C_{xz} \\ 0 & i_y & 0 \\ -C_{xz} & 0 & i_z \end{bmatrix}, i = \{r, f\}$

APPENDIX B
VEHICLE PARAMETERS

See Tables 4–6.

REFERENCES

[1] *Rokon Website*. Accessed: Jun. 5, 2020. [Online]. Available: https://www.rokon.com/

[2] *Öhlins Website*. Accessed: Jun. 5, 2020. [Online]. Available: https://www.ohlins.com/

[3] *Christini Technologies Website*. Accessed: Jun. 5, 2020. [Online]. Available: https://www.christini.com/awd-technology/about-the-technology

[4] M. Blundell and D. Harty, *The Multibody System Approach to Vehicle Dynamics*. Oxford, U.K.: Butterworth-Heinemann, 2004.

[5] D. J. N. Limebeer and R. S. Sharp, "Bicycles, motorcycles and models," *IEEE Control Syst. Mag.*, vol. 26, no. 5, pp. 34–61, Oct. 2006.

[6] R. S. Sharp, "The stability and control of motorcycles," *J. Mech. Eng. Sci.*, vol. 13, no. 5, pp. 316–329, Oct. 1971.

[7] K. K. Cooper, "The effect of aerodynamics on the performance and stability of high speed motorcycles," Nat. Aereonautical Establishment, National Research Council of Canada, Ottawa, ON, Canada, 1974.

[8] R. S. Sharp, "The stability of motorcycles in acceleration and deceleration," in *Proc. Inst. Mech. Eng. Conf. Braking Road Vehicles*, London, U.K., 1976, pp. 45–50.

[9] D. J. N. Limebeer, R. S. Sharp, and S. Evangelou, "The stability of motorcycles under acceleration and braking," *Proc. Inst. Mech. Eng., C, J. Mech. Eng. Sci.*, vol. 215, no. 9, pp. 1095–1109, Sep. 2001.

[10] R. S. Sharp and D. J. N. Limebeer, "A motorcycle model for stability and control analysis," *Multibody Syst. Dyn.*, vol. 6, no. 2, pp. 123–142, 2001.

[11] R. S. Sharp, "The application of multi-body computer codes to road vehicle dynamics modelling problems," *Proc. Inst. Mech. Eng., D, J. Automobile Eng.*, vol. 208, no. 1, pp. 55–61, Jan. 1994.

[12] H. B. Pacejka and R. S. Sharp, "Shear force development by pneumatic tyres in steady state conditions: A review of modelling aspects," *Vehicle Syst. Dyn.*, vol. 20, nos. 3–4, pp. 121–176, 1991.

[13] E. J. H. de Vries and H. B. Pacejka, "Motorcycle tyre measurements and models," *Vehicle Syst. Dyn.*, vol. 29, no. 1, pp. 280–298, Jan. 1998.

[14] Y. Tezuka, H. Ishii, and S. Kiyota, "Application of the magic formula tire model to motorcycle maneuverability analysis," *JSAE Rev.*, vol. 22, no. 3, pp. 305–310, Jul. 2001.

[15] H. B. Pacejka, *Tire Vehicle Dynamics*. Oxford, U.K.: Butterworth-Heinemann, 2012.

[16] V. Cossalter and R. Lot, "A motorcycle multi-body model for real time simulations based on the natural coordinates approach," *Vehicle Syst. Dyn.*, vol. 37, no. 6, pp. 423–447, Jun. 2002.

[17] R. Lot and V. Cossalter, "A nonlinear rider model for motorcycles," in *Proc. FISITA World Automot. Cong.*, Yokohama, Japan, Jan. 2006, pp. 1–11.

[18] R. Lot, M. Massaro, and R. Sartori, "Advanced motorcycle virtual rider," *Vehicle Syst. Dyn.*, vol. 46, no. sup1, pp. 215–224, Sep. 2008.

[19] A. Saccon, J. Hauser, and A. Beghi, "A virtual rider for motorcycles: An approach based on optimal control and maneuver regulation," in *Proc. 3rd Int. Symp. Commun., Control Signal Process.*, Mar. 2008, pp. 243–248.

[20] J. D. G. Kooijman and A. L. Schwab, "A review on bicycle and motorcycle rider control with a perspective on handling qualities," *Vehicle Syst. Dyn.*, vol. 51, no. 11, pp. 1722–1764, Nov. 2013.

[21] S. Hima, L. Nehaoua, N. Seguy, and H. Arioui, "Suitable two wheeled vehicle dynamics synthesis for interactive motorcycle simulator," in *Proc IFAC World Cong.*, Seoul, South Korea, 2008, vol. 41, no. 2, pp. 96–101.

[22] L. Nehaoua, H. Arioui, N. Seguy, and S. Mammar, "Dynamic modelling of a two-wheeled vehicle: Jourdain formalism," *Vehicle Syst. Dyn.*, vol. 51, no. 5, pp. 648–670, May 2013.

[23] A. Bonci, R. De Amicis, S. Longhi, E. Lorenzoni, and G. A. Scala, "Comparison of dynamic models for a motorcycle during lowside fall," *WSEAS Trans. Appl. Theor. Mech.*, vol. 12, pp. 78–85, Jan. 2017.

[24] J. W. Griffin and A. A. Popov, "Multibody dynamics simulation of an all-wheel-drive motorcycle for handling and energy efficiency investigations," *Vehicle Syst. Dyn.*, vol. 56, no. 7, pp. 983–1001, Jul. 2018.

[25] S. Evangelou, *Control and stability Analysis of Two-Wheeled Road Vehicle*. London, U.K.: Univ. London, 2004.

[26] T. Abumi and T. Murakami, "Posture stabilization of two-wheel drive electric motorcycle by slip ratio control considering camber angle," in *Proc. IEEE Int. Conf. Mechatronics (ICM)*, Mar. 2015, pp. 353–358.

[27] J. Ben, B. V. Aswin, R. Adityan, and G. T. Basil, "Two wheel drive motorcycle," *IOSR J. Mech. Civil Eng.*, vol. 11, no. 1, pp. 25–32, 2014.

[28] S. Mammar, S. Glaser, and M. Netto, "Vehicle lateral dynamics estimation using unknown input proportional-integral observers," in *Proc. Amer. Control Conf.*, Jun. 2006, p. 6.

[29] Y. Sebsadji, S. Glaser, S. Mammar, and M. Netto, "Vehicle roll and road bank angles estimation," *Proc. 17th World Congr. Int. Fed. Autom. Control Seoul*, South Korea, 2008, pp. 7091–7097.

[30] A. Bonci, R. De Amicis, S. Longhi, G. A. Scala, and A. Andreucci, "Motorcycle lateral and longitudinal dynamic modeling in presence of tyre slip and rear traction," in *Proc. 21st Int. Conf. Methods Models Autom. Robot. (MMAR)*, Aug. 2016, pp. 391–396.

[31] S. M. Savaresi and M. Tanelli, *Active Braking Control Systems Design for Vehicles*. London, U.K.: Springer-Verlag, 2010.

[32] S. M. Savaresi, C. Poussot-Vassal, C. Spelta, O. Sename, and L. Dugard, *Semi-active Suspension Control Design for Vehicles*. Oxford. U.K.: Elsevier, 2010.

[33] V. Cossalter, *Motorcycle Dynamics*, Morrisville, NC, USA: Lulù.com, 2006.

[34] A. Bonci, R. De Amicis, S. Longhi, E. Lorenzoni, and G. A. Scala, "A motorcycle enhanced model for active safety devices in intelligent transport systems," in *Proc. 12th IEEE/ASME Int. Conf. Mech. Embedded Syst. Appl. (MESA)*, Aug. 2016, pp. 1–6.

[35] *MSC Adams Tyre Software Manual*. Accessed: Jun. 27, 2018. [Online]. Available: https://simcompanion.mscsoftware.com/infocenter/index?page=content&channel=DOCUMENTATION&cat=1VMO50

[36] A. Bonci, R. De Amicis, S. Longhi, E. Lorenzoni, and G. A. Scala, "Motorcycle's lateral stability issues: Comparison of methods for dynamic modelling of roll angle," in *Proc. 20th Int. Conf. Syst. Theory, Control Comput. (ICSTCC)*, Oct. 2016, pp. 13–15.

ANDREA BONCI (Member, IEEE) holds the position of an Assistant Professor in automatic control and the Head of the Automation Laboratory, Università Politecnica delle Marche. His research interests include modeling and control of dynamic systems, system and control theory, vehicle dynamics, automotive systems, modeling and control of autonomous systems, mechatronic, robotics, embedded systems applications, industrial automation, cyber-physical systems, and smart manufacturing.

SAURO LONGHI (Senior Member, IEEE) holds the positions of a Full Professor in robot technologies and a Rector at the Università Politecnica delle Marche. His main research interests include modeling, identification and control of linear and nonlinear systems, control of mobile robots, service robots for assistive applications supporting mobility and cognitive actions, home and building automation, and automatic fault detection and isolation.

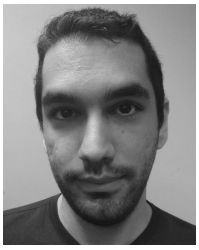

GIUSEPPE ANTONIO SCALA received the master's degree in computer and automation engineering from the Università Politecnica delle Marche, in 2018, where he is currently pursuing the Ph.D. degree in automation engineering with the Dipartimento di Ingegneria dell'Informazione. His main research interests include robotics, nonlinear system analysis and control, virtual simulations, and computer science.